Numerical simulation of the melting process of nanostructured based colloidal suspensions phase change materials including the effect of the transport of the particles

El Hasadi, Yousef M.F.

Important note
To cite this publication, please use the final published version (if applicable).
Please check the document version above.

Numerical simulation of the melting process of nanostructured based colloidal suspensions phase change materials including the effect of the transport of the particles

Yousef M.F. El Hasadi

Process and Energy Department, Delft University of Technology, Leeghwaterstraat 39, 2628, CB, Delft, the Netherlands

ABSTRACT

Nanostructured phase change materials (NEPCM) colloidal suspensions, got the attention from the scientific community due to their promising thermal properties that allow for faster solidification, and melting times. However, most of the experimental investigation shows the opposite, that the melting and freezing times are increased as the volume of the particles is increased. This investigation will be the first in the literature to include the mass transport of the particles, for the case of melting of NEPCM that will help understanding better the melting process of the NEPCM. In this paper, the development of the solid-liquid interface, the distribution of the nanoparticle profiles, as well as the development of the thermal convection, will be investigated for the case of melting of nanostructured phase change materials (NEPCM) colloidal suspensions, inside a rectangular cavity. The numerical model is based on the one-fluid-mixture approach combined with the single-domain enthalpy-porosity model for phase change. The linear dependence of the liquids, and solidus temperatures with the concentration of the nanoparticles was assumed. The NEPCM consists of water and copper nanoparticles, the nanoparticle size was selected to be 5 nm and 2 nm. The suspension was melted inside a rectangular cavity, heated from the left side. It was observed that for the case of dp = 2 nm, as the mass fraction of the particles increases the solid-liquid interface changes from a planar to unstable morphology during melting. Furthermore, as the mass fraction of the particles increases the temperature of the suspension decreased similarly to experimental observations. Also, I found that the rate of the rejection of the particles and the particles size plays an essential role in the development of the liquid fraction, concentration field, and the resulted thermal convection.

© 2019 Published by Elsevier B.V.

1. Introduction

Nanostructured phase change materials (i.e., NEPCM) are colloidal suspensions that emerged as a substitute for the single component phase changes materials. Because, of their higher thermal conductivity, that results from suspending of highly thermal conductive structures such as nanoparticles [1–3], carbon nanotubes [4–6], graphene [7], and carbon nanofibers [8–9]. As a phase change material, the NEPCM will undergo melting and solidification cycles, during those cycles' particles will be rejected out from the emerging phase, because of thermo-dynamic constraints [10]. The early numerical models that have been used to investigate the solidification and melting process of those newly proposed phase change materials are continuum-based models that treat the NEPCM as a single-phase mixture [11–13]. In those models, the effect of the particles is only included in the thermophysical properties, and thus those models do not count for the mass transport of the particles, which is essential for real-life simulations. By using those

theoretical frameworks, solidification and melting times will always decrease with increasing the volume fraction of the particles due to the increase in thermal conductivity. However, the experimental observations reveal an unexpected behavior that the decrease of the melting and freezing times is not monotonic with the increase of the volume fraction of the particles [1,15]. Recently, El Hasadi and Khodadadi [16,17] developed a continuum model that consider the transport of the particles for the simulation of the freezing process of colloidal suspensions. They were the first to predict the emergence of a dendritic shape for the solid-liquid interface, which reassembles the experimental observations for the freezing of colloidal suspensions and the NEPCM [18,19]. They come into the conclusion that increasing the volume fraction of the particles will not always decrease the freezing time. They showed that the rejection of the nanoparticles played an essential role in determining the operational conditions in which the expedited freezing of the NEPCM, will occur.

Most of the investigations that deals with the melting of the nanostructure phase change materials (NEPCM) are experimental. The experiments showed that, at the beginning of the melting process, the primary mechanism that controls heat transfer is conduction, While,

Nomenclature

c_p	Specific heat (J/kgK)
C_m	Porosity constant (kg/m^{3}s)
d_p	Particle diameter (nm)
D_B	Brownian diffusion (m^2/s)
D_T	Thermophoretic diffusion (m^2/s)
$\vec{e}_y$	Unit vector in the y-direction
H	Length of the cavity (m)
k	Thermal conductivity (W/mK)
k_0	Segregation coefficient
k_B	Boltzmann constant (J/K)
L	Latent heat (J/kg)
m_l	Liquidus slope (K)
p	Pressure (Pa)
t	Time (s)
T	Temperature (K)
$\vec{U}$	Velocity vector (m/s)
v_p	Volume of the particle (m^3)
x, y	Cartesian coordinates (m)

Greek symbols

α	Thermal diffusivity (m^2/s)
ρ	Density (kg/m^3)
μ	Dynamic viscosity (Pa·s)
λ	Liquid fraction of colloid
φ	Volume fraction of particles
φ_w	Weight or mass fraction of particles

Subscripts

c	Cold
f	Base fluid
h	Hot
in	Initial conditions
l	Liquid
Liq	Liquidus
p	Particle
s	Solid
Sol	Solidus

sedimentation observed at the end of each experiment. Zeng et al. [14] investigated the melting performance of NEPCM, which consisted of carbon nanotubes (8–15 nm in diameter) suspended in 1-dodecanol PCM. The mass fraction of the nanotubes suspended was ranged between 1 and 2% by mass. The suspension was melted inside a rectangular cavity form the bottom side. They found that during the early stage of melting where the heat transfer is controlled by conduction. The temperature readings for the samples that contain 1 and 2% by mass nanoparticles were higher than those of the pure PCM. They attributed that to the higher thermal conductivity for the samples containing carbon nanotubes. However, as the melting proceeds further the trend is reversed and temperature for the pure PCM case is increasing much faster than the ones that consist of carbon nanotubes, they attribute this behavior because of the higher enhancement in viscosity than that of the thermal conductivity which helped to degrade the strength of the natural convection. Their viscosity and thermal conductivity measurements are consistent with their argument. The observations of [1,14] conflict with the numerical results of [11–13] since the numerical simulations showed that enhancement in the melting rate could be achieved for particle loadings of >2% by volume. However, for most experiments, the improvement in melting rates was observed in much lower loadings about <0.6% by volume as in [2]. This discrepancy was attributed due to lack of real thermophysical property measurements, and appropriate constitutive laws that govern the real behavior of NEPCM.

Modeling the transport of the particles during the melting process of the NEPCM is necessary to understand in more depth the physics that accompanies the melting process. For the best of my knowledge, no one investigated before or attempted to include the mass transport of the particles during the melting of colloidal suspensions. For this reason. I will investigate the melting behavior of copper-water colloidal suspension NEPCM inside a rectangular cavity. The effects of different parameters such as the mass fraction of the particles, different values of the segregation coefficients (i.e., which represents the ratio between the concentration of the particles in the solid and liquid phases respectively), and particle sizes. Will be examined to elucidate their role in the development of the solid-liquid interface, convection pattern, and concentration field. In particular, this investigation will help to shed more light on the reports from the experiments that the temperature is decreasing as the volume of the particles is increased.

2. Mathematical modeling

Colloidal suspensions such as NEPCM consisted of nanoparticles can be considered as binary mixtures, and during their melting process, a mushy zone will develop due to the difference between the solidus and liquidus temperatures. A mushy zone is a region where within its boundaries, the solid and liquid phases coexist, and the phase transition occurs. Due to the similarity of the behavior between the colloidal suspensions used in the current investigation and those of binary mixtures, the numerical model that I will use to simulate the melting process of the NEPCM has its roots on the one-fluid mixture model. The one-fluid mixture model is used widely to simulate the solidification process of binary alloys as shown in [20]. The principal assumptions of the current model are the following:

1. The thermophysical properties of the solvent (i.e., water) are isotropic and equal for both the solid and liquid phases.
2. The liquid and solid phases in the mushy zone are always at thermodynamic equilibrium state.
3. The pulling velocity was assumed to be zero, which results in a stationary solid phase.
4. The density of the fluid in the gravitational force term is changing according to the Boussinesq approximation, accounting for the

as the melting processes progress in time, the heat-transfer mechanism switches form conduction to natural convection. In most of the experimental investigations for the NEPCM, observations show that as the volume fraction of the particles increases, it results in the suppression of natural convection, which results in the prolongation of the melting process. The primary explanation for the suppression of the natural convection was attributed due to the greater enhancement of the viscosity compared to that of the thermal conductivity. For example, Ho and Gao [1] conducted melting experiments for a NEPCM consisted of n-octadecane and alumina nanoparticles, with the mass fraction of the particles ranging from 0 to 10%. The colloidal suspension is melted inside a square container heated isothermally from its vertical sides. They observed that the Nusselt number at the hot side of the cavity followed the trend seen during the melting experiments of pure phase change materials [2].

Furthermore, they observed that as the mass fraction of the particles increased the value of the Nusselt number decreased compared to that of the pure octadecane for the whole range of operating conditions used in their experiments. The authors argued that the decrease in the Nusselt number and thus in the heat transfer rate may be attributed to two factors. The first one is the significant increase of viscosity of the suspension with the increase of the mass fraction of the particles, and the second one may be due to the considerable amount of particle

thermal-solutal effects due to the change of the density with temperature and the concentration of the particles.

5. The thermophysical properties of the suspension are changing with the concentration of the particles.

2.1. Governing equations

The transport of momentum, energy and mass transfer of the particles equations are valid for both thermodynamic phases of liquid, solid, and in the mushy zone as well. The dimensional volume averaged equations for the case of NEPCM are the following:

Continuity:

$$\nabla \cdot \overrightarrow{U} = 0, \tag{1}$$

Momentum:

$$\rho \frac{\partial \overrightarrow{U}}{\partial t} + \rho \left(\overrightarrow{U} \cdot \nabla \right) \overrightarrow{U} = -\nabla p + \mu \nabla^2 \overrightarrow{U} - \rho \frac{C_m (1-\lambda)^2}{\lambda^3} \overrightarrow{U} + (\rho \beta) g \left(T - T_{ref} \right) \overrightarrow{e}_y \tag{2}$$

Thermal energy

$$\rho c_p \frac{\partial T}{\partial t} + \rho c_p \overrightarrow{U} \cdot \nabla T = \nabla \cdot (k \nabla T) - \rho L \frac{\partial \lambda}{\partial t} \tag{3}$$

Species:

$$\frac{\partial \phi_w}{\partial t} + \overrightarrow{U} \cdot \nabla \phi_w = \nabla \cdot \left(D_B \nabla \phi_w + D_T \frac{\nabla T}{T} \right) \tag{4}$$

where $\overrightarrow{U}, T$ and, ϕ_w, are the velocity vector, temperature, and the mass fraction of the particles. With the local values of the particle mass fraction (ϕ_w) and colloid liquid fraction (λ) related through the following relation:

$$\phi_w = \lambda \phi_{wl} + (1-\lambda)\phi_{ws} \tag{5}$$

The momentum equations consist of the Darcy Law damping terms, and the related porosity constant C_m was set to a value of 10^5 kg/m³ s Furthermore, the impact of the nanoparticle diffusion to the heat flux vector in the energy equation is neglected [21].

Fig. 1. Geometry of the physical model.

2.2. Initial/boundary conditions

The geometry of the physical model considered in the present investigation is a square cavity (side H) containing the colloidal suspension (NEPCM) as shown in Fig. 1. The melting of the suspension is initiated by increasing the temperature of the left side of the cavity (T_H) above the liquidus temperature corresponding to the initial concentration, while the right vertical side was kept at a constant temperature ($T_C = 271$ K). The remaining two horizontal sides are kept thermally insulated. The initial conditions implemented for all the cases, considered in the current paper are the following:

$$\overrightarrow{U}_{in} = 0, T_{in} = 272K \tag{6}$$

for $t = 0$

The mass fraction of the particles varies between 0, 0.05, and 0.1.

2.3. Mixture relations and effective thermophysical/transport properties

The colloidal suspension used consists of hard sphere particles, with the assumption that particle clusters do not form. The properties of the solvent (i.e. water) in the liquid and solid phases are kept constant (i.e. the density effect is neglected). However, all the thermophysical properties of the colloidal suspension change with the volume fraction (ϕ) of the particles. Density of the NEPCM, heat capacities and part of the Boussinesq terms are calculated from the mixture relation:

$$\rho = (1-\varphi)\rho_f + \varphi \rho_p$$

$$\rho c_p = (1-\varphi)(\rho c_p)_f + \varphi (\rho c_p)_p,$$

$$\rho \beta = (1-\varphi)(\rho \beta)_f + \varphi (\rho \beta)_p. \tag{7c}$$

where β is the thermal expansion coefficient, the mass fraction can be converted to the corresponding volume fraction via the following relation:

$$\phi = \frac{\rho_f \phi_w}{\rho_f \phi_w + \rho_p (1-\phi_w)} \tag{8}$$

The viscosity of the NEPCM is obtained from:

$$\mu = \frac{\mu_f}{(1-\phi)^{2.5}} \tag{9}$$

The thermal conductivity of the NEPCM suspension is evaluated using:

$$k = k_1 + k_2 \tag{10a}$$

that combines the Maxwell relation:

$$k_1 = k_f \frac{k_p + 2k_f - 2\phi (k_f - k_p)}{k_p + 2k_f + \phi (k_f - k_p)} \tag{10b}$$

and the enhancement due to thermal dispersion given by:

$$k_2 = C_k (\rho c_p) \left| \overrightarrow{U} \right| \phi d_p \tag{10c}$$

C_k represents an empirical constant obtained from Wakao and Kaguei [22]. To account for the effect of the volume fraction, on the mass diffusivity of the of the particles (Brownian diffusivity), a
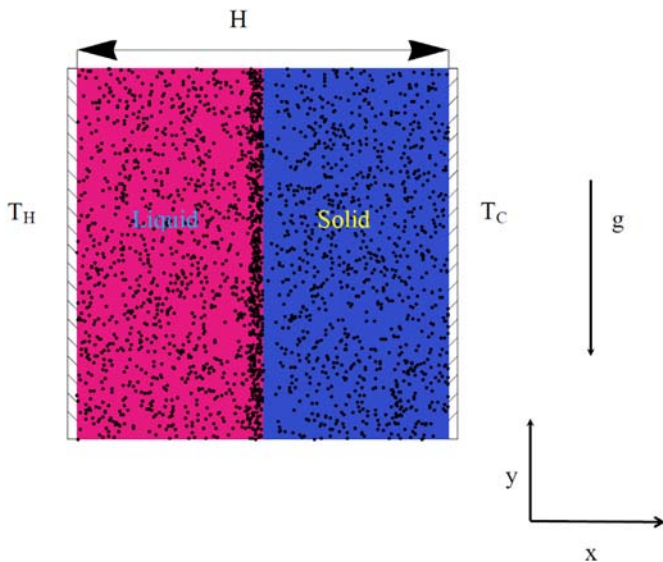
compressibility factor is calculated from empirical fitting as recommended by [23]:

$$z(\phi) = \frac{1 + \left(4 - \frac{1}{0.64}\right)\phi + \left(10 - \frac{4}{0.64}\right)\phi^2 + \left(18 - \frac{10}{0.64}\right)\phi^3}{1 - \frac{\phi}{0.64}}$$ (11a)

The mass diffusivity of the particles as function of the volume fraction is given by the following:

$$D_B = D_o(1-\phi)^6\left(\frac{d(\phi z)}{d\phi}\right)$$ (11b)

where D_0 is calculated from the Einstein-Stokes relation:

$$D_0 = \frac{Tk_B}{3\pi d_p\mu}$$ (11c)

The thermophoretic diffusivity is computed from the following relation:

$$D_T = \beta_k\left(\frac{\mu}{\rho}\right)\phi$$ (12)

where $\beta_k = 0.26(\frac{k_f}{2k_f + k_p})$ is a nondimensional parameter that is a function of the thermal conductivities of base liquid and the nanoparticle as it is suggested by Buongiorno [21]. Sensible enthalpy and latent heat of fusion make up the enthalpy of the NEPCM and the latent heat is calculated from the following relation:

$$\rho L = (1-\phi)(\rho L)_f$$ (13)

The current mathematical model utilizes the change of the of liquidus and solidus temperatures, with the concentration of the nanoparticles which is a fundamental feature of binary mixture melting. A linear phase diagram has been chosen for the current investigation since the initial concentration used is in the dilute limit. The liquids and solidus temperatures are given by Eqs. (14a) and (14b) obtained from [23]:

$$T_{Liq} = T_m - m_l\phi_w,$$

$$T_{Sol} = T_m - \frac{m_l}{k_0}\phi_w,$$ (14b)

where T_m, m_l and k_0 represent the melting temperature of the pure solvent (in this case water taken as 273 K), the liquidus slope and the segregation coefficient, respectively. The segregation coefficient represents the ratio between mass fraction of the particles on the solid and liquid sides of the solid-liquid interface. The liquidus temperature of NEPCM is dependent inversely with the volume of the particle and thus their size. As shown in the following relation that specially developed for NEPCM [23]:

$$m_l = \frac{k_BT_m^2}{v_p\rho L_f}$$ (15)

The value of the segregation coefficient (k_0) kept constant to the value of 0.1 for the whole simulation period.

The colloid liquid fraction (λ) is related to the local liquidus and solidus temperatures via the following relations:

$$\lambda = 0 \qquad for\ T < T_{Sol},$$
$$\lambda = \frac{T - T_{Sol}}{T_{Liq} - T_{Sol}} \quad for\ T_{Sol} < T < T_{Liq}, \lambda = 1 \qquad for\ T > T_{Liq}.$$ (16)

The mixture model utilized here has been extensively used for simulating binary alloy solidification problems [20,24]. In the present study, the applicability and relevance of this model is extended to the melting problem of colloidal suspensions of nano-scale particles. For more information about the mathematical formulations that govern the transport properties the reader is advised to refer to ground breaking investigations of El Hasadi and Khodadadi [16,17].

3. Solution procedure

The discretization method of choice for the governing equations was the finite volume method. A staggered grid was selected, with the x and, y grids are uniformly distributed. The SIMPLE algorithm was used to handle the coupling of the pressure and the velocity fields. The enthalpy porosity method was used to simulate the melting process. Handling the coupling between the convection and diffusion terms for the momentum, energy, and species equations were done by using the second-order upwind scheme. The enthalpy porosity method was used to simulate the melting process. The implemented convergence criterion required that at the end of each time step the residuals of the momentum equation be lower than 10^{-5}, whereas for energy and species equations this value was 10^{-7}. The variable time step was set to 0.01 s for 1000time steps, then increased to 0.05 s for another 1000 time steps and finally raised to 0.1 s for the remainder of the simulation. To implement the numerical algorithm the computational fluid dynamics software FLUENT was used. The variation of the thermophysical properties with the concentration of the particles, and the temperature of the suspension achieved by implementing specially designed user-defined functions. The results of the adopted model were also compared to those of Hannoun et al. [25] for the case of melting of pure tin inside a rectangular cavity heated on the vertical walls. Comparing Fig. 2(a) to (b) it is observed that the present model adequately captures the presence of a single recirculating cell at time instant $t = 100$ s and its breakdown to a multi-cell structure at $t = 200$ s. Our results matched the tabulated results for the solid-liquid interface of [25] at the same time instances (Fig. 2e), the details of the current model are listed in [16]. There are several other numerical verification studies for the case of NEPCM melting [26–30] for the interested reader A grid independence study was conducted using grid arrangements of 50×50, 100×100 and 150×150. The 100×100 grid system was selected due to its accuracy and reduced simulation time as shown in Fig. 2d.

4. Results and discussion

In the current section, the results of the present numerical investigations will be discussed. Emphasis will be given to the effect of the segregation coefficient, mass fraction of the particles, and particle size on the melting process of the NEPCM. The properties of the nanoparticles and the solvent are listed in Table 1. The governing non-dimensional parameters for the case of the pure water are the following Stefan number(St) = $\frac{c_p(T_H - T_C)}{L} = 0.099$, Rayleigh number $(Ra) = \frac{\rho\beta g(T_H - T_C)H^3}{\mu\alpha} = 1.8 \times 10^5$, and the segregation coefficient (k_0), the values of St, and Ra will not change significantly since the concentration of the particles is in the extreme dilute regime.

Fig. 2. Comparison between the results of the current model and [25]: (a) stream function at $t = 100$ s (current model), (b) stream function for $t = 200$ s (current model) and (c) instantaneous positions of the liquid-solid interfaces. (d) grid independence test for different grid sizes.

(a)

(d)

(b)
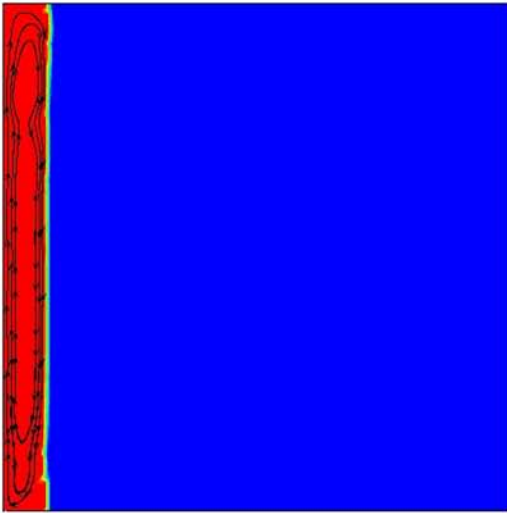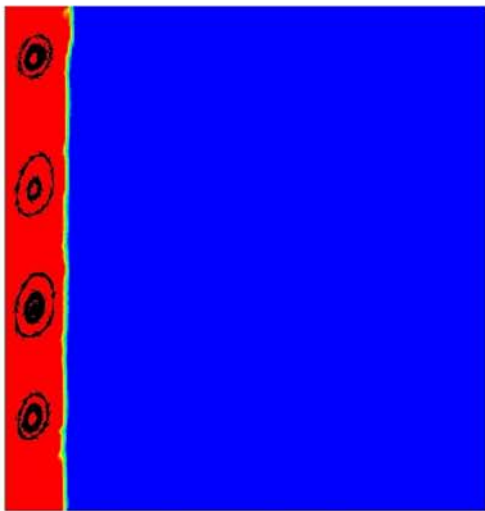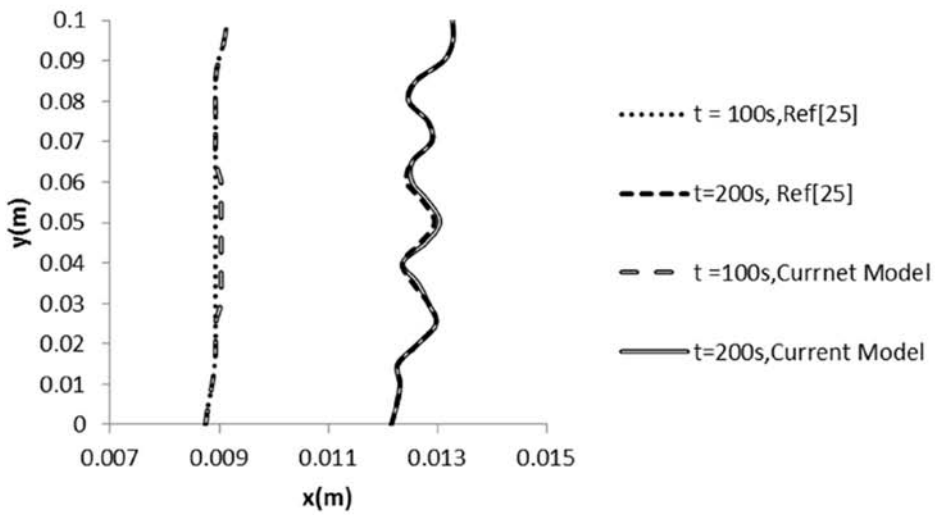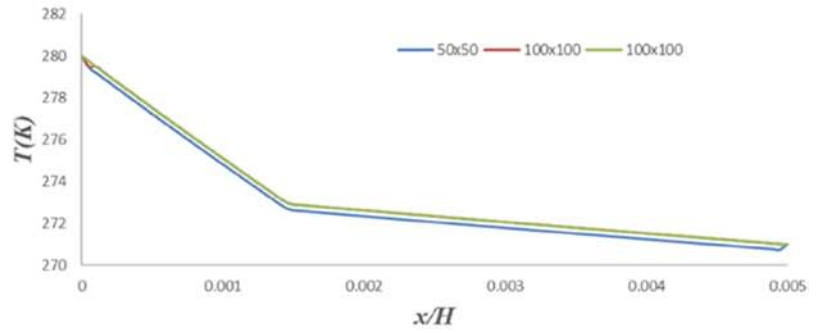
(c)

4.1. Development of the liquid fraction and concentration profiles

The transient development of the superimposed liquid fraction, stream lines and concentration of the particles profiles for the case of copper-water colloidal suspension (NEPCM) with a particle size of $d_p = 2$ nm, $\phi_w = 10\%$, $k_0 = 0.1$, and $T_H = 280$ K are presented in Figs. 3 and 4, respectively.

At the beginning of the melting process Fig. 3a ($t = 10s$), the solid-liquid interface is planar. The flow consists of a weak counterclockwise cell that occupies the melted part of the suspension as shown by the streamlines. As the melting process proceeds, the solid-liquid interface is developing from planar to non-planar shape due to the increase in the strength of convection currents as shown in Fig. 3b ($t = 100$ s). Furthermore, the mushy zone (where the solid and liquid phases coexist) developed. The formation of the mushy zone comes as a result of the alternation of the solidus and liquidus temperatures due to the redistribution of the concentration of the nanoparticles as shown in Eqs. (14a) and (14b). Within the mushy zone, the regions with higher particles concentration are melted faster in comparison with lower concentration regions, because the melting temperature decreases with the increase of particles concentration, similar to the binary alloy. The dependence of the melting temperature on the concentration leads to the formation of solid branches and solid islands surrounded by a liquid phase in the mushy zone. The solid channels are regions with a higher melting temperature since they are the regions with particle concentration. Thus, it will melt slower than the surrounding liquid that consists of a higher concentration of particles as shown in Fig. 4. The flow cell increases in size and strength, as the melting process proceeds further as in Fig. 3c and d ($t = 250$ s, and 500 s), the solid-liquid interface took a curved shape due to the high intensity of the natural convection, especially in the upper part of the cavity. The center of the flow cell is moved downward further with time.

Because of the thermodynamic constraints, the solid phase will reject particles in the liquid melt [10]. Evidence of the sedimentation of particles during melting is reported in the experiments of [1,2,and 7] which results in a concentration gradient near the interface. For this purpose, the mass distribution of the particles has been investigated for the similar conditions as those of Fig. 3. Which, shows that as the time proceeds, the concentration of the particles in the liquid melt increases as shown in Fig. 4a, due to the rejection of the particles from the solid phase, however, due to the convection in the melt the particles redistributed nearly uniformly in the liquid part of the suspension. As the time proceed further, the particles are redistributed mostly in the region near the interface as shown in Fig. 4b, and Fig. 4c with the high concentration of the particles is concentrated in the space between the solid channels.

4.2. The effect of the mass fraction of the particles

One of the critical parameters that shape the performance of the nanostructured phase change materials is the transport of the mass fraction of the particles. For this purpose, three different loadings of particles had been selected $\phi_w = 0$, 5, and 10% by mass. The segregation coefficient for all the runs will be kept constant, and its value will be 0.1, and the hot temperature will be adjusted to $T_H = 280$ K. The solid-liquid interface for the cases of $\phi_w = 0\%$, and 5% developed a curved shape resulted from the effect of the convection that formed as shown in Fig. 5a, and Fig. 5b. Furthermore, the solid phase was melted nearly with a uniform temperature since the mass fraction of the particles is small and thus the solidus and liquidus temperatures will not significantly vary. However, as the mass fraction of the particles increased to 10%, the solid phase is no more melted at a uniform temperature, but now its melting temperature depends strongly on the concentration of the particles, which results in a non-stable shape of the interface as shown from Fig. 5c. In order, to elucidate further the effect of the concentration of the particles on the development of the liquid fraction. I

Table 1
Thermophysical and transport properties for the solvent and the nanoparticles.

	Water	Copper nanoparticles
Density	997.1 kg/m³	8954 kg/m³
Viscosity	8.9×10^{-4} Pa s	–
Specific heat	4179 J/kg K	383 J/kg K
Thermal conductivity	0.6 W/m K	400 W/m K
Thermal expansion coefficient [16]	2.1×10^{-4} K^{-1}	1.67×10^{-5} K^{-1}
Heat of fusion	3.35×10^5 J/kg	–

will plot the temporal evolution of the ratio between the average liquid fraction for the NEPCM to that of the pure solvent (water,$\phi_w = 0$)

$$\lambda_r = \frac{\bar{\lambda}_{\phi,k_0}}{\bar{\lambda}_{\phi=0}} \qquad (17)$$

Fig. 6 shows the transient development of λ_r for the cases discussed in Fig. 5. It shows that the growth of the liquid fraction for the case of $\varphi_w = 0.1$ is faster than the pure case (i. e. $\varphi_w = 0.0$). This expatiated behavior can be attributed due to the decrease of the melting temperature with the concentration, rather than due to the increase of the thermal conductivity resulted from the suspension of the particles. Furthermore, the expediting rate is decreasing with time. As for the case of $\phi_w = 0.05$, shows no expediting behavior in comparison with that of pure water (i. e. $\phi_w = 0.0$) where in the opposite it shows deceleration. The streamlines from Fig. 5 shows that the velocity flow structure is quite similar for the three considered. To further illustrate the effect of the mass fraction on the velocity field, I will plot the ratio between the maximum stream function for the suspension to that of the solvent (Eq. (18)) as a function of time as shown in Fig. 7.

$$\psi_{r1} = \frac{\psi\big|_{\max,\varphi_w,k_0}}{\psi\big|_{\max,\varphi_w=0.0}} \qquad (18)$$

The value of ψ_{r1} for the case of $\phi_w = 0.05$ is nearly unity, which shows that the velocities for the suspension and the pure solvent are nearly equal($\psi_{r1} \approx 1$). However, as the mass fraction increases to $\phi_w = 0.1$, ψ_{r1} changes nonlinearly with time. At the early stages of melting, the values of the maximum stream function for the suspension (with $\phi_w = 0.1$) is 7% higher than that of the pure solvent, however, as the time elapsed further the value of ψ_{r1} attains a local minimum, which is now 3% below that of the pure solvent. As time increases further, the velocity strength of the suspension enhanced compared to that of the solvent ($\psi_{r1} > 1$). Fig. 7 shows that convection strength during melting increases nonlinearly with the mass fraction of the particles.

To illustrate further the effect of the mass fraction of the particles in the melting process of the nanostructured phase change materials (NEPCM) the temperature profiles along the horizontal axis located at the middle of the vertical side of the duct are shown in Fig. 8. The patterns are quite similar near the hot side of the cavity. However, near the solid-liquid interface the temperature values for suspension with $\phi_w = 0.1$ are lower compared to the temperature values for the suspensions with $\phi_w = 0.0$, and 0.05 respectively. These observations are qualitatively consistent with the experimental measurements of [1,7] which they show that the temperature readings are decreased as the mass fraction of the particles is increased. Which let them to concluded that the growth of the solid-liquid interface is decelerated. However, no experimental study tracked the solid-liquid interface visually for the case of the NEPCM. Because the colloidal suspensions are opaque solutions, which are extremely difficult to see through them. Thus, the lower temperature values cannot be conclusive as for where the solid-liquid interface is decelerated or not as we show in the current investigation, because the melting temperature is strongly dependent on the concentration of the particles.
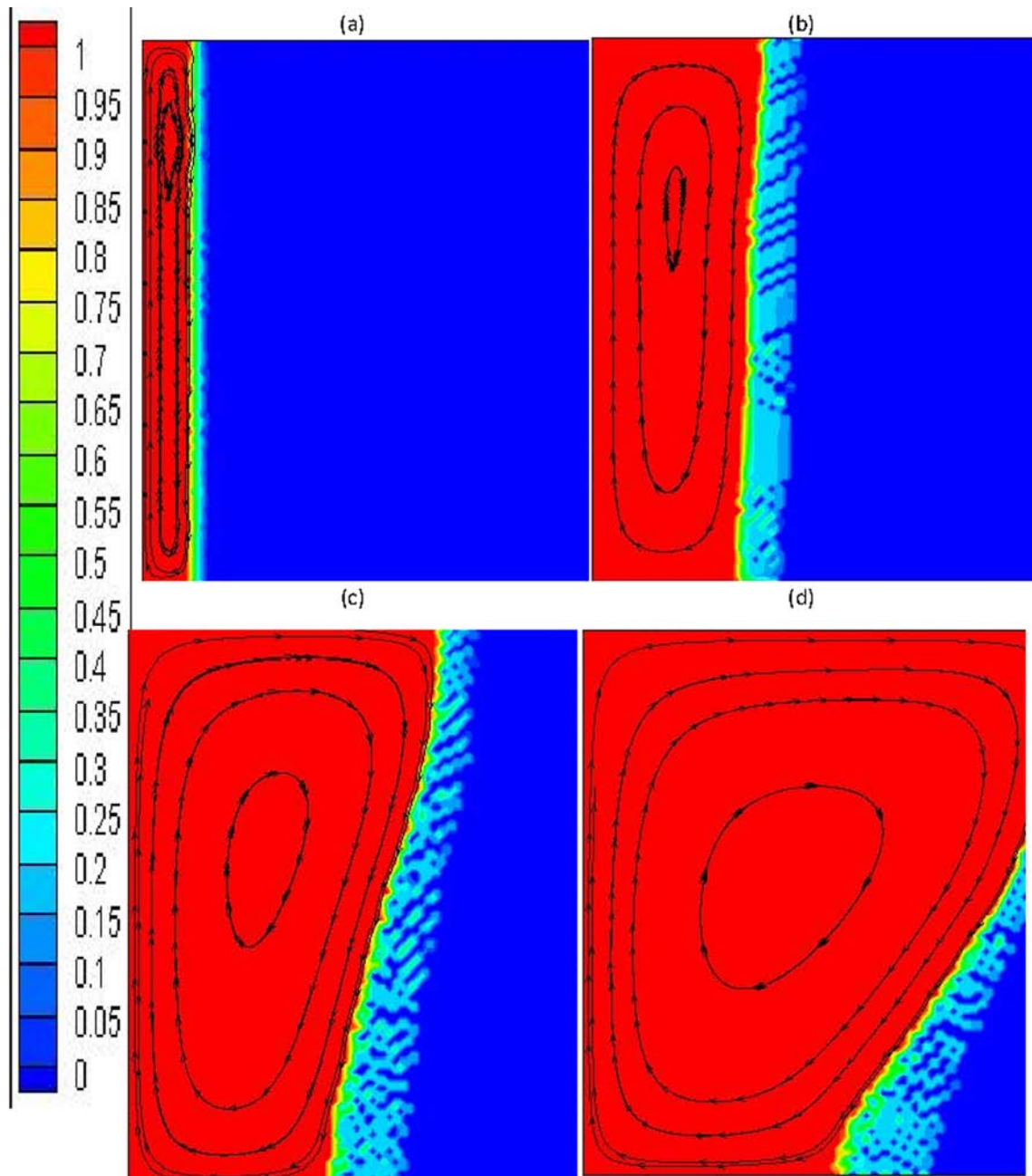
Fig. 3. Development of the flow field (shown by the streamlines) superimposed on the contours of the liquid fraction for, copper nanoparticles of $d_p = 2$ nm at (a) t = 10 s, (b) t = 100 s, (c) $t = 250$ s, and (d) $t = 500$ s.

4.3. The effect of the segregation coefficient (k_0)

One of the main contributions of the current paper to the scientific literature is the investigation of the particle transport during the melting process. The main parameter in the current model that controls the rejection of the particles is the segregation coefficient (k_0), its value can range from 1.0 (which represents the case of no particles been rejected) to zero (all the particles been rejected), the segregation coefficient is strongly depend on the velocity of the solid-liquid interface, the particle size, type, and volume fraction. However, for the sake of simplicity we will assume that the segregation coefficient is constant. I have chosen the following values for $k_0 = 1.0$, and 0.1, where the former represents a case with no particle rejection, while the later represents a case with substantial particle rejection. The following operational conditions of $T_H = 280$ K, $T_C = 271$ K, $d_p = 2$ nm, and $\phi_w = 0.1$ are chosen.

Superimposed contours of the liquid fraction and the streamlines for $k_0 = 1.0$ and 0.1 are shown in Fig. 9. For the case of $k_0 = 1.0$ (Fig. 9a), the solid-liquid interface developed a stable curved shape, similar shapes are observed for the cases of melting of a single component material. This can be explained that for the case of $k_0 = 1.0$, the particles will not be redistributed, and the suspension will melt with a uniform temperature similarly to that of the single component material. However, for the case of $k_0 = 0.1$, which represents a case with significant particle rejection, and the particles will redistribute throughout the melted NEPCM. This will change the liquidus and solidus temperatures. This will help the formation of unstable solid-liquid interface as in Fig. 9b. For further illustration of the effect of the segregation coefficient (k_0) on the development of the solid-liquid interface, the parameter λ_r has been plotted for the two cases investigated in this section as shown in Fig. 10. For the case of $k_0 = 1.0$, the transient behavior of λ_r is nonlinear
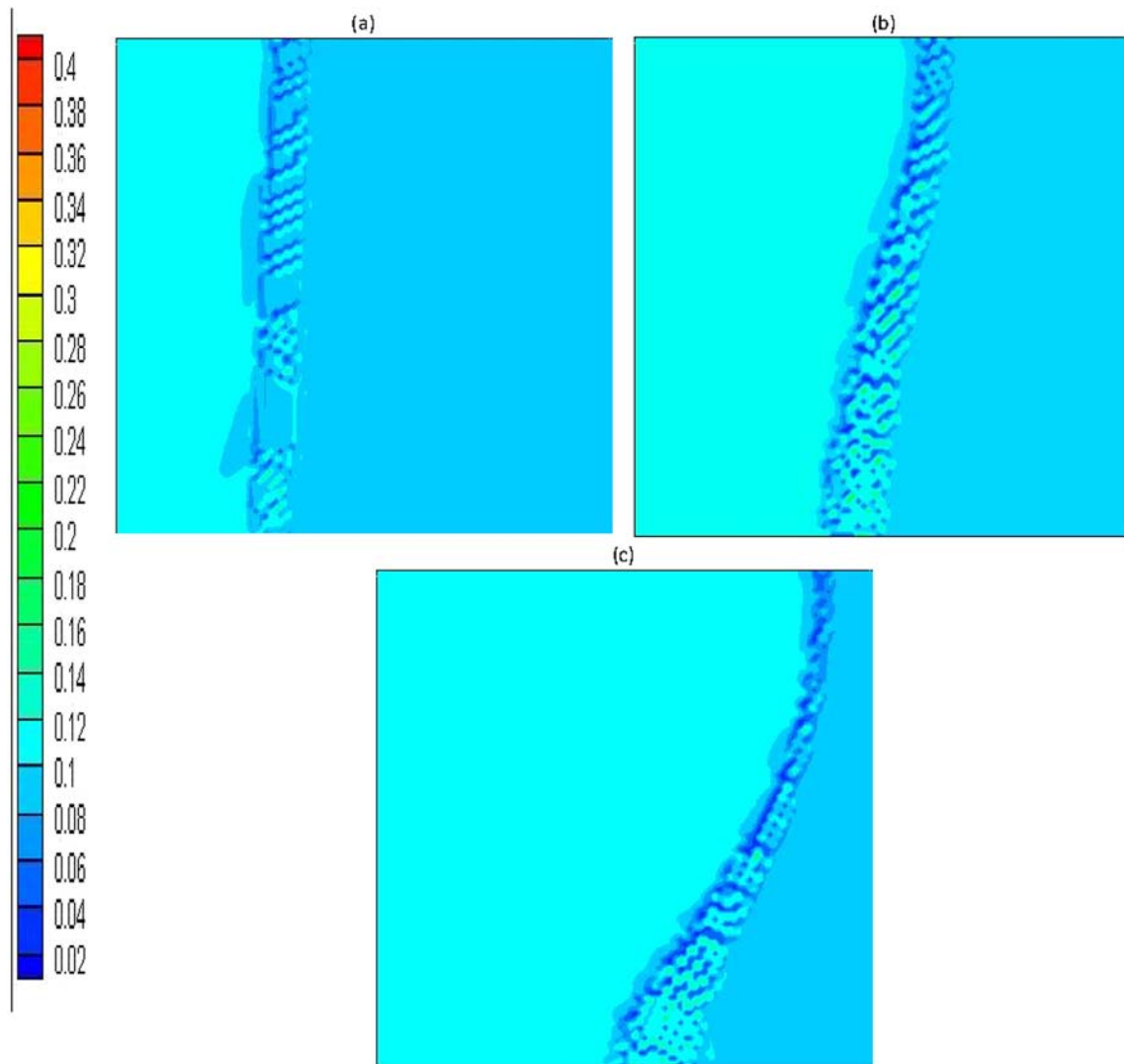
Fig. 4. Development of the concentration field for with, copper nanoparticles of $dp = 2$ nm at different time instants, (a) $t = 100$ s, (c) $t = 250$ s, and (d) $t = 500$ s.

since its value increases at the early stages of the melting process and then attains maximum value, and then decreases. The values of λ_r were below unity, which means that the pure solvent (i.e. water) melted faster than the water copper suspension with $k_0 = 1.0$. However, for the case of $k_0 = 0.1$, the values of λ_r were always greater than unity, which means that when the rejection of the particles included within the modeling process of the melting, the suspension melted faster than the pure solvent (i.e. water), and it is linearly decreasing with time.

Fig. 9 shows also the streamlines of the flow, and for the both cases, the flow is consisted from a single circulation for both cases $k_0 = 1.0$, and 0.1. However, for the better illustration of the effect of the segregation coefficient on the velocity filed the parameter ψ_{r1} has been plotted with respect to time for the two cases of $k_0 = 1.0$, and 0.1 as shown in Fig. 11. The values of ψ_{r1} for the case of $k_0 = 1.0$ are always increases with time, which indicates that the strength of the flow is increasing with time. However, for the case of $k_0 = 0.1$ the values of ψ_{r1} attain a local minimum and then increases. For the both cases, the values of ψ_{r1} increase beyond one at the late stages of the melting, this indicates that the strength of the flow, for the case of the suspensions is higher than that of the pure water. The values of ψ_{r1} for the case of $k_0 = 0.1$ are higher than that of the case of $k_0 = 1.0$ at the early stages of the melting. However, the trend is reversed as the time proceeds further until the late stage of the melting is reached, then the values of ψ_{r1} for

the two cases are nearly equal. The expiated melting behavior for the case of $k_0 = 0.1$ can be explained mainly due to the lowering of the liquidus temperature, not due to the increase of the convection. Since, for the most part, of the melting process the convection strength for the case of $k_0 = 0.1$ is lower than that of $k_0 = 1.0$.

4.4. The effect of the size of the particles

In this section, we will investigate the effect of the particle on the melting process of NEPCM. The diameter of the particles plays an essential role on how fast the particles will diffuse, and how much the liquidus and solidus temperatures will change as shown in Eq. (11b) and (15) respectively. For this purpose, I will use two different sizes $d_p = 5$ nm, and 2 nm. The other operational parameters are kept with the following values $\phi_w = 0.1$, k0 = 0.1, $T_H = 280$ K, and $T_C = 271$ K.

The transient development of the superimposed contours of the streamlines and the liquid fraction for the two particle sizes considered in the current investigation are shown in Fig. 12. For the case of $d_p = 5$ nm $t = 100$ s, the solid-liquid interface has a planar shape which indicates that conduction is the governing heat transfer mechanism (Fig. 12a). However, for the case of $d_p = 2$ nm the solid-liquid interface had an unstable morphology, and mushy zone region started to form, for the reasons that been explained in detail in Section 4.1. As the time proceeds further, the solid-liquid interface for the case of $d_p = 5$ nm
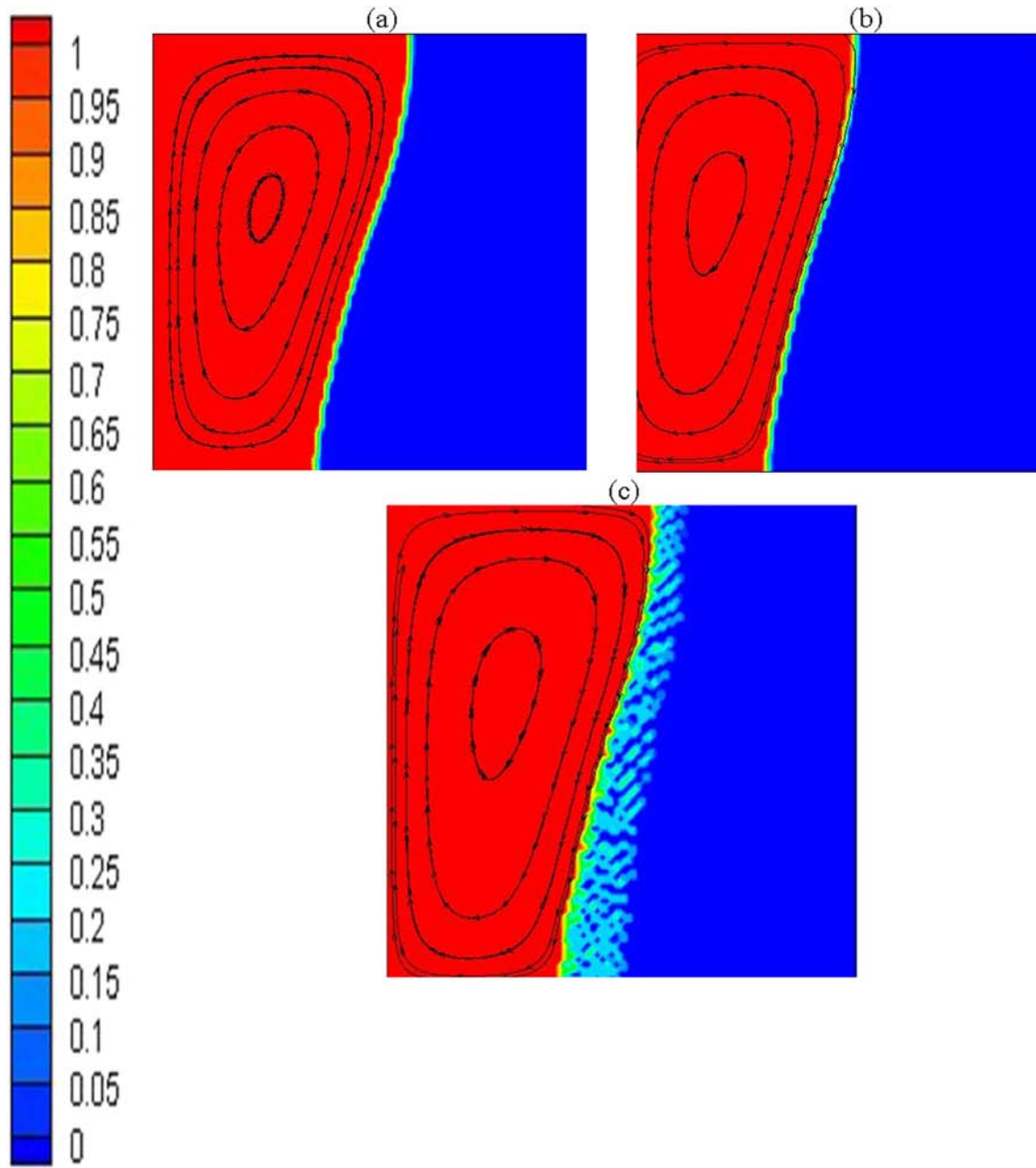
Fig. 5. Superimposed contours of streamlines and liquid fraction at $t = 250$ s for $T_H = 280$ K, $d_p = 2$ nm and for (a) $\varphi_w = 0.00$ and (b) $\varphi_w = 0.05$, and (c) $\varphi_w = 0.1$.
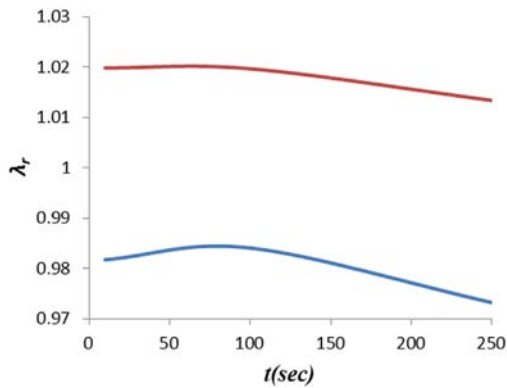
Fig. 6. The transient development of λ_r for different mass fractions of particles (φ_w), $d_p = 2$ nm.
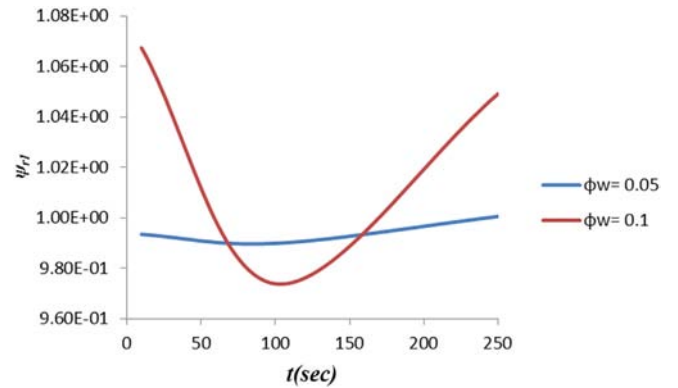
Fig. 7. The transient development of ψ_{r1} for different mas fraction of the particles, and for $d_p = 2$ nm.
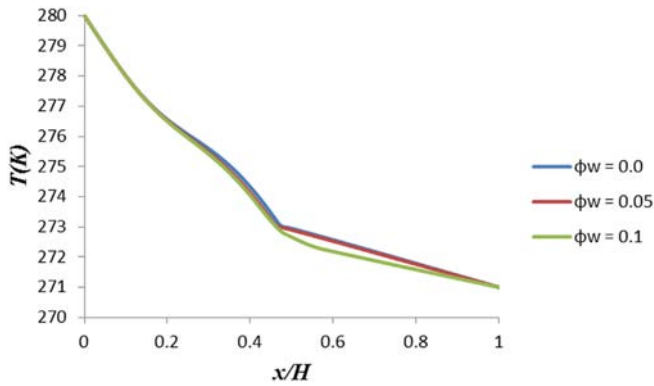
Fig. 8. Temperature profile at $y = 0.5H$ and, along the x- axis for $d_p = 2$ nm.
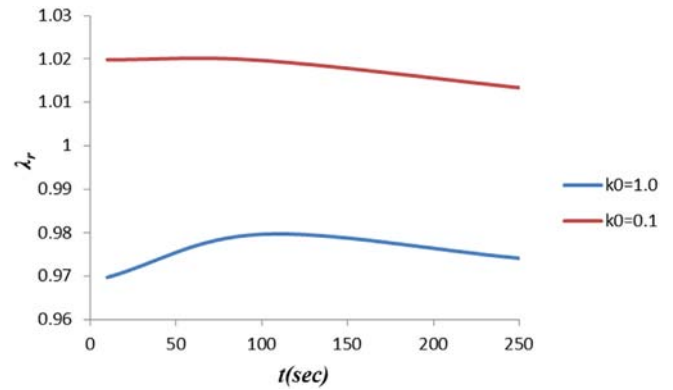
Fig. 10. The transient development of λ_r for different segregation coefficients, $\varphi_w = 0.1$, and $d_p = 2$ nm.

formed a curved shape due to the increase in temperature in the upper part of the cavity because the strength of the convection increased at that region (Fig. 12c). As for the case of $d_p = 2$ nm, the solid-liquid interface formed a curved unstable morphology (Fig. 12d). Fig. 12 showed that the particle size plays an essential role in the resulted morphology of the interface. To measure the influence of adding particles of different sizes on the increase of the melting rate of the NEPCM. The transient parameter λ_r was plotted as shown in Fig. 13. From Fig. 13, it is clearly shown that the suspension with dp =2 nm showed an expedited behavior if it compared to that of the pure solvent during the time the whole span of the simulation. While, for the case of dp =5 nm, the behavior is the opposite, the melting rate is decelerated concerning the pure solvent during the same period of the simulation.

The flow filed for both particle sizes consists of a single cell, which occupies the melting portion of the suspension as shown in Fig. 12a to 12d. The effect of the particle size on the strength of the convection formed during melting is shown by plotting the transient variation of ψ_{r1} for the two particle sizes $d_p = 5$ nm, and 2 nm as shown in Fig. 14. It clearly that for the significant part of the simulation time, the convection strength for the case of $d_p = 2$ nm is higher than that of $d_p = 5$ nm. Moreover, the transient variation of ψ_{r1} for $d_p = 2$ nm is nonlinear while that for $d_p = 5$ nm is linearly increasing with time. We see this behavior because for the case of $d_p = 2$ nm, the diffusion coefficient is higher than in the case of $d_p = 5$ nm, and thus the particles will be redistributed

more effectively for the former case rather than later one, this redistribution seems to affect the strength of the convection.

5. Conclusions

For the first time, a numerical investigation of the melting problem of NEPCM is presented including the transport of the particles. The main goals of the current investigation are to elucidate the effects of the segregation coefficient, mass fraction of the particles, and particle size on the melting process of the suspension. There are significant new findings that help to understand more deeply the evolution of the meting process of colloidal suspensions. Here are some of the most important conclusions and findings:

1- As the mass fraction of the particles increases the NEPCM showed an expedited melting compared to the pure solvent (i. e. water), for the case of $d_p = 2$ nm. The decrease in the melting time is attributed to the decrease of the melting temperature with the increase of the concentration of the particles, rather due to the increase of the thermal conductivity of the suspension.

2- The variation of the relative convection strength with the mass fraction of the particles for the $d_p = 2$ nm case is non-monotonic throughout the simulation. However, the predominate observation
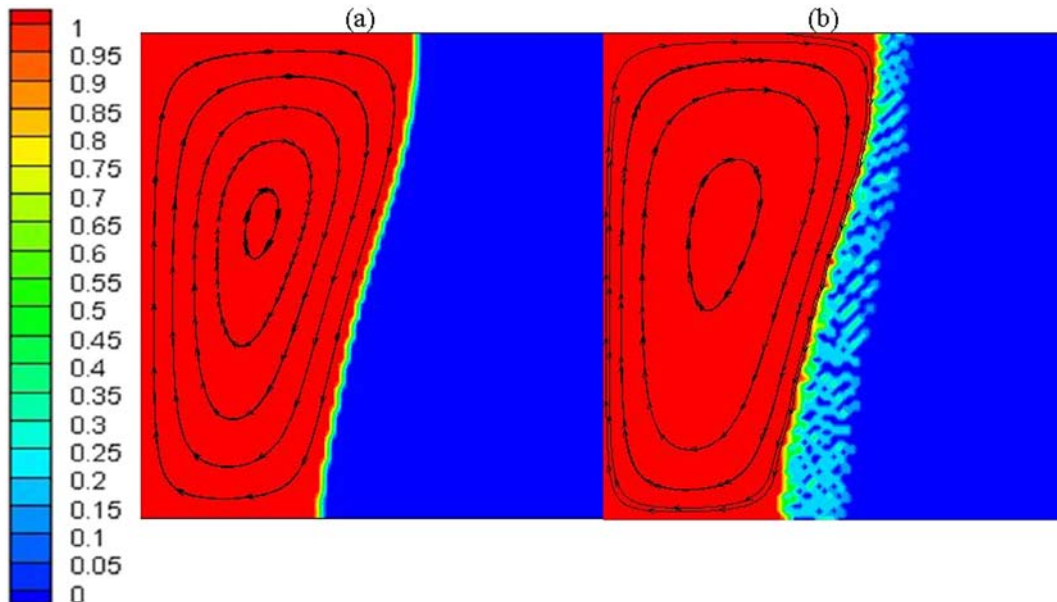
Fig. 9. Superimposed contours of streamlines and liquid fraction at $t = 250$ s for $T_H = 280$ K, $\varphi_w = 0.1$, $d_p = 2$ nm and for (a) $k_0 = 1.0$ (b) $k_0 = 0.1$.
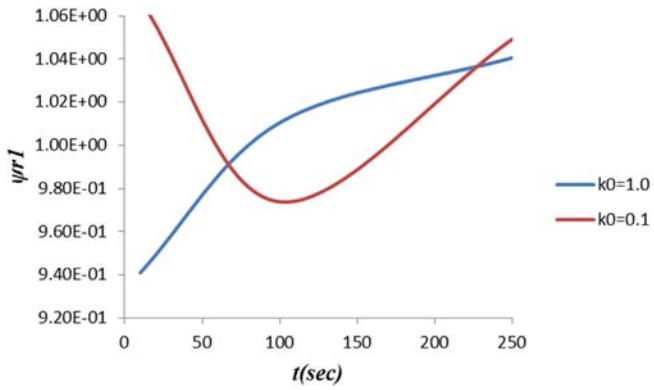
Fig. 11. The transient development of ψ_{r1} for different segregation coefficients, $\varphi_w = 0.1$ and for $d_p = 2$ nm.
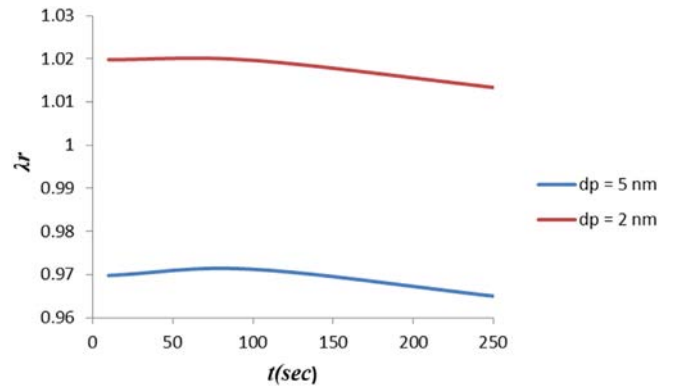
Fig. 13. The transient development of λ_r for different particle sizes, $\varphi_w = 0.1$, and $k_0 = 0.1$.
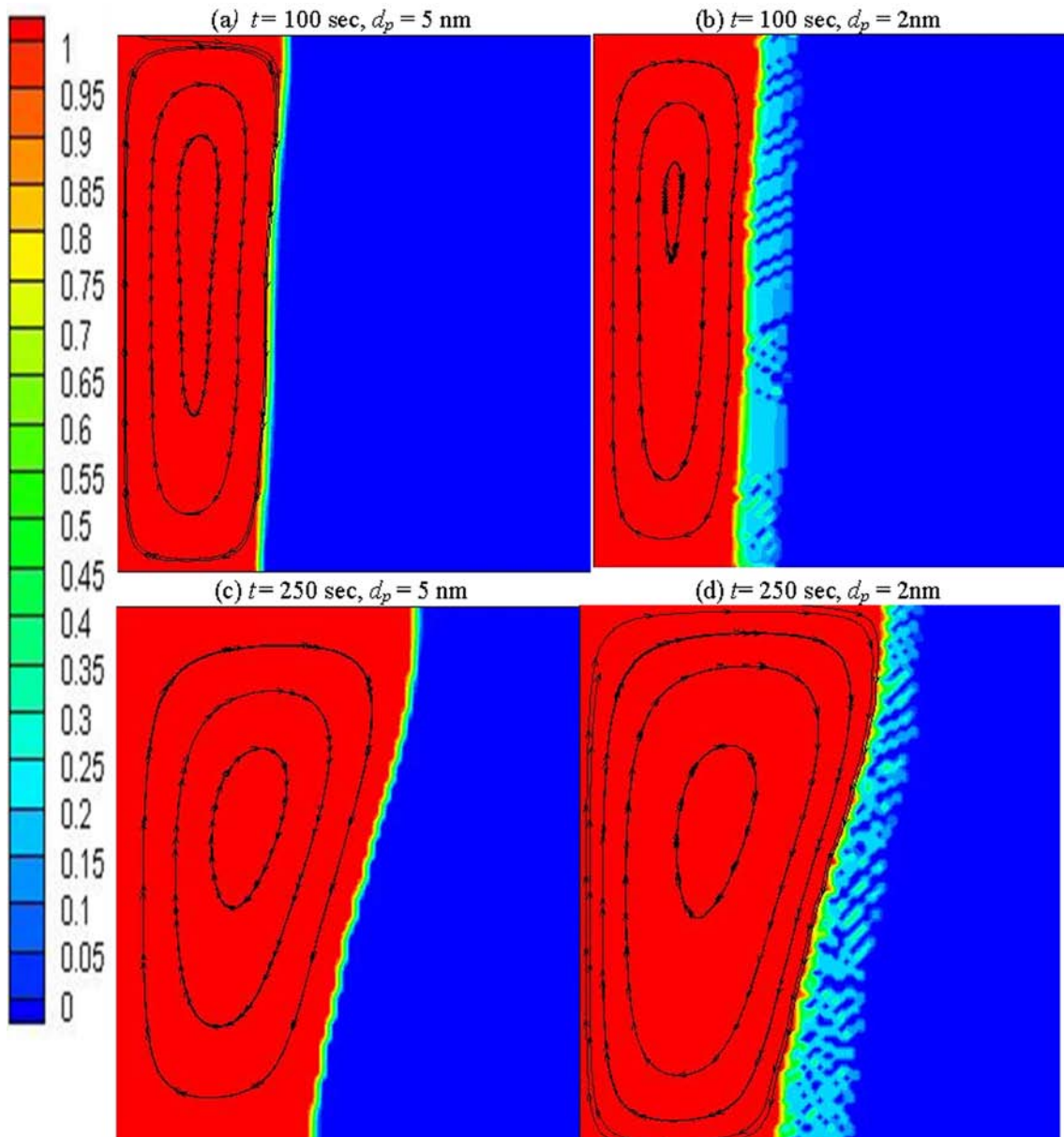
Fig. 12. Superimposed contours of streamlines and liquid fraction at for $T_H = 280$ K, $\varphi_w = 0.1$, $k_0 = 0.1$, at different time instances and particle sizes.
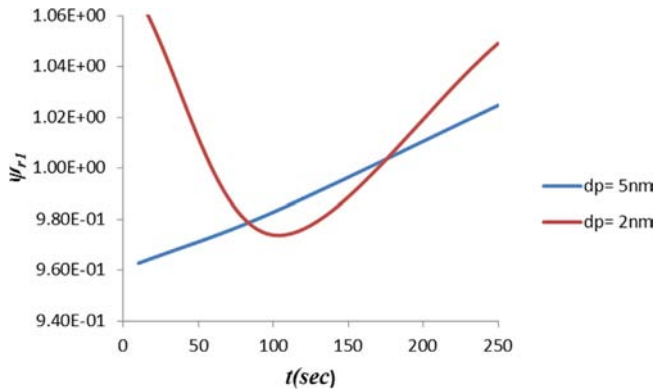
Fig. 14. The transient development of ψ_{r1} for different particle sizes, $\varphi_w = 0.1$, and $k_0 = 0.1$.

is that for the most significant part of the simulation, the suspension with $\phi_w = 0.1$ exhibit's convection currents with higher strength than that of the $\phi_w = 0.05$.

3- For the case of $d_p = 2$ nm as the mass fraction of the particles increases, the temperature of the suspension decreases. This temperature decrease is similar to the observations of the experiments, where they reported a significant decrease in temperature readings.

4- For the case of $d_p = 2$ nm, as the segregation coefficient decreases the suspension melts faster than the pure solvent, because its melting temperature was decreased due to the particle transport.

5- The reduction of the particle size helps to accelerate the melting process of the NEPCM.

6- The convection strength for the case of $d_p = 2$ nm is higher than that of $d_p = 5$ nm, in the most significant part of the simulation.

The current investigation showed how complex the melting process of the NEPCM is, and in how many parameters it depends. However, further investigation is needed especially on developing mathematical correlations for the different transport properties. I believe that Stokesan dynamics [31] type of simulation for obtaining the viscosity and the diffusion of the suspensions in a more fundamental way because those properties are the ones with the more dominant effect for the case of melting, rather than the thermal conductivity.

Acknowledgment

References

[1] C.J. Ho, J.Y. Gao, An experimental study on melting heat transfer of paraffin dispersed with $Al_2 O_3$ nanoparticles in a vertical enclosure, Int. J. Heat Mass Transf. 62 (2013) 2–8.
[2] N.S. Dhaidan, J.M. Khodadadi, T.A. Al-Hattab, S.M. Al-Mashat, Experimental and numerical investigation of melting of phase change material/nanoparticle suspensions in a square container subjected to a constant heat flux, Int. J. Heat Mass Transf. 66 (2013) 672–683.
[3] C.J. Ho, J.Y. Gao, Preparation and thermophysical properties of nanoparticle-in-paraffin emulsion as phase change material, Int. Commun. Heat Mass Transfer 36 (5) (2009) 467–470.
[4] Y. Cui, C. Liu, S. Hu, X. Yu, The experimental exploration of carbon nanofiber and carbon nanotube additives on thermal behavior of phase change materials, Sol. Energy Mater. Sol. Cells 95 (4) (2011) 1208–1212.
[5] J. Wang, H. Xie, Z. Xin, Y. Li, L. Chen, Enhancing thermal conductivity of palmitic acid based phase change materials with carbon nanotubes as fillers, Sol. Energy 84 (2) (2010) 339–344.
[6] Ye, F., Ge, Z., Ding, Y., & Yang, J. (2013), "Multi-walled carbon nanotubes added to Na_2CO_3/MgO composites for thermal energy storage". Particuology.
[7] X. Fang, L. Fan, Q. Ding, X. Wang, X. Yao, J. Hou, ... K. Cen, Increased thermal conductivity of eicosane-based composite phase change materials in the presence of graphene nanoplatelets, Energy Fuel 27 (2013) 4041–4047.
[8] O. Sanusi, R. Warzoha, A.S. Fleischer, Energy storage and solidification of paraffin phase change material embedded with graphite nanofibers, Int. J. Heat Mass Transf. 54 (2011) 4429–4436.
[9] A. Elgafy, K. Lafdi, Effect of carbon nanofiber additives on thermal behavior of phase change materials, Carbon 43 (15) (2005) 3067–3074.
[10] Dantzig, J. A., and Rappaz M., Solidification, 2009, EPFL Press.
[11] S.F. Hosseinizadeh, A.R. Darzi, F. Tan, Numerical investigations of unconstrained melting of nano-enhanced phase change material (NEPCM) inside a spherical container, Int. J. Therm. Sci. 51 (2012) 77–83.
[12] A.A. Ranjbar, S. Kashani, S.F. Hosseinizadeh, M. Ghanbarpour, Numerical heat transfer studies of a latent heat storage system containing nano-enhanced phase change material, Therm. Sci. 15 (2011) 169–181.
[13] S. Kashani, A.A. Ranjbar, M. Abdollahzadeh, S. Sebti, Solidification of nano-enhanced phase change material (NEPCM) in a wavy cavity, Heat Mass Transf. 48 (2012) 1155–1166.
[14] Y. Zeng, L.W. Fan, Y.Q. Xiao, Z.T. Yu, K.F. Cen, An experimental investigation of melting of nanoparticle-enhanced phase change materials (NePCMs) in a bottom-heated vertical cylindrical cavity, Int. J. Heat Mass Transf. 66 (2013) 111–117.
[15] L. Fan, J.M. Khodadadi, A theoretical and experimental investigation of unidirectional freezing of nanoparticle-enhanced phase change materials, J. Heat Transf. 134 (9) (2012).
[16] Y.M. EL Hasadi, J.M. Khodadadi, Numerical simulation of the effect of the size of suspensions on the solidification process of nanoparticle-enhanced phase change materials, J. Heat Transf. 135 (5) (2013).
[17] Y.M. El Hasadi, J.M. Khodadadi, One-dimensional Stefan problem formulation for solidification of nanostructure-enhanced phase change materials (NePCM), Int. J. Heat Mass Transf. 67 (2013) 202–213.
[18] S.S. Peppin, M.G. Worster, J.S. Wettlaufer, Morphological instability in freezing colloidal suspensions, Proc. Royal Soc. 463 (2007) 723–733.
[19] S.N. Schiffres, S. Harish, S. Maruyama, J. Shiomi, J.A. Malen, Tunable electrical and thermal transport in ice-templated multi–layer graphene nanocomposites through freezing rate control, ACS Nano 7 (2013) 11183–11189.
[20] C. Beckermann, R. Viskanta, Double-diffusive convection during dendritic solidification of binary mixture, PCH Physicochem. Hydrodyn. 10 (1988) 195–213.
[21] J. Buongiorno, Convective transport in nanofluids, Journal of Heat Transfer-T ASME 128 (2006) 240–251.
[22] N. Wakao, S. Kaguei, Heat and Mass Transfer in Packed Beds, Gordon and Breach Science Publishers, New York, NY, 1982 175–205.
[23] S.S. Peppin, J.A. Elliott, M.G. Wroster, Solidification of colloidal suspensions, J. Fluid Mech. 554 (2006) 147–166.
[24] V.R. Voller, C. Prakash, Fixed grid numerical modeling methodology for convection-diffusion mushy region phase change problems, Int. J. Heat Mass Transf. 30 (1987) 1709–1719.
[25] N. Hannoun, V. Alexiades, T.Z. Mai, A reference solution for phase change with convection, Int. J. Numer. Methods Fluids 48 (2005) 1283–1308.
[26] M. Jourabian, M. Farhadi, K. Sedighi, A.A.R. Darzi, Y. Vazifeshenas, Melting of NEPCM within a cylindrical tube: numerical study using the lattice Boltzmann method, Numerical Heat Transfer, Part A: Applications 61 (12) (2012) 929–948.
[27] M. Jourabian, M. Farhadi, A.A.R. Darzi, Outward melting of ice enhanced by Cu nanoparticles inside cylindrical horizontal annulus: lattice Boltzmann approach, Appl. Math. Model. 37 (20−21) (2013) 8813–8825.
[28] M. Jourabian, M. Farhadi, K. Sedighi, On the expedited melting of phase change material (PCM) through dispersion of nanoparticles in the thermal storage unit, Comput. Math. Appl. 67 (7) (2014) 1358–1372.
[29] M. Jourabian, M. Farhadi, A.A. Rabienataj Darzi, Accelerated melting of PCM in a multitube annulus-type thermal storage unit using lattice Boltzmann simulation, Heat Transfer Asian Res. 46 (8) (2017) 1499–1525.
[30] M. Jourabian, M. Farhadi, A.R. Darzi, Constrained ice melting around one cylinder in horizontal cavity accelerated using three heat transfer enhancement techniques, Int. J. Therm. Sci. 125 (2018) 231–247.
[31] J.F. Brady, G. Bossis, Stokesian dynamics, Annu. Rev. Fluid Mech. 20 (1) (1988) 111–157.